Jurnal Kejuruteraan 38(3) 2026: 1237-1251
https://doi.org/10.17576/jkukm-2026-38(3)-19

A New Class of Wavelength/Time/Spatial 3-D FCC-MDW Code for Cardinality Enrichment in OCDMA Networks

Abu Jubaer Rupok[a], C.B.M. Rashidi[a*], K.N.F. Ku Azir[a], Xiaoli Chu[b], Mohammad Nayeem Morshed[c] & B.Nakarmi[d*]

[a]*Centre of Excellence for Advanced Computing, Faculty of Intelligent Computing, Universiti Malaysia Perlis, Kampus Alam, 02600, Arau, Perlis, Malaysia.*

[b]*School of Electrical and Electronic Engineering, University of Sheffield, Sheffield, United Kingdom.*

[c]*ICT Cell, Islamic University, Kushtia, Bangladesh.*

[d]*Nanjing University of Aeronautics and Astronautics, Nanjing, Jiangsu, China*

[*]*Corresponding author: rashidibeson@unimap.edu.my & bikash@nuaa.edu.cn*

Received 3 September 2025, Received in revised form 14 December 2025
Accepted 14 January 2026, Available online 30 May 2026

ABSTRACT

This paper presents a new class of three-dimensional (3-D) flexible cross-correlation modified double-weight (FCC-MDW) optical code-division multiple access (OCDMA) codes. Existing 1-Dimensional and 2-Dimensional OCDMA codes face challenges such as high interference, limited number of users, and increased complexity. The proposed 3-D FCC-MDW code addresses these problems by integrating FCC and MDW coding properties in the wavelength, time and spatial-domains spreading, resulting in high number of users, better interference suppression, and optimum optical received power at receiver part. In contrast to traditional coding methods, the 3-D FCC-MDW code achieves minimal cross-correlation and high spectral efficiency while maintaining low complexity in design. While providing a BER of $10^{-9}$and a transmission speed of 1.25 Gbps, the 3-D FCC-MDW OCDMA code is capable of supporting 310 users, corresponding to user capacity improvements of 3.9 times, 5.2 times, and 3.1 times over the 3D-multi-diagonal code, 3D-Single weight zero cross-correlation (ZCC), and 3D-Variable weight ZCC, respectively. Moreover, the performance is attained at a received power of -24 dBm, representing a 29 dB power saving compared with the other approaches. Additionally, the proposed code achieves superior spectral efficiency, requiring only 0.084 THz of bandwidth compared with up to 5.67 THz used by existing schemes. Transmission experiments confirm long-distance performance, providing reliable transmission over 100 km without amplification and achieving a BER as low as 1.54×10^{-10}. These results show that the 3-D FCC-MDW is a highly efficient, power-optimized, and scalable solution for future fiber-optic communication networks.

Keywords: 3 -dimensional; FCC; MDW; OCDMA; MAI; BER; PIIN

INTRODUCTION

In the Optical Code Division Multiple Access (OCDMA) systems, users are distinguished by unique codewords rather than assigned time slots or wavelengths, as employed in conventional Time-Multiplexing systems and Wavelength-Multiplexing systems, respectively. This coding-based approach enables multiple users to access the communication channel both intermittently and simultaneously (Nlend & Swart, 2023). Over the years, various single-domain (1D) and bi-dimensional (2D) OCDMA coding techniques have been explored. In 2D coding schemes (Cherifi et al. 2021), optical pulses are spread jointly across time and frequency domains, assigning distinct time chips to different wavelengths. In contrast, 1D codes (Alayedi et al. 2024) distribute optical chips solely in either the time or wavelength domain. Early OCDMA research primarily focused on 1D encoding (Boukricha et al. 2020), but it was quickly recognized that enhancing the system's user capacity in a 1D system requires longer code lengths, which in turn increases

system complexity and cost. To address these limitations, researchers have investigated the design of zero cross-correlation (ZCC) codes (Kumari & Bansal, 2023), which effectively eliminate MAI and improve system performance. This advancement was conducted to the development of 2D encoding systems (Aljunied et al. 2021), including wavelength/spatial, wavelength/time, and time/polarization (T/P) configurations (Liang et al. 2023). Numerous 2D codes have been proposed based on varied mathematical frameworks such as eigenvalues, identity matrices, and changing properties. However, even with 2D encoding (Mizozoe et al. 2023), enhancing user capacity generally necessitates longer temporal or spatial sequences, depending on the adopted code construction method. A higher number of users often translates to longer spatial spreading or extended time slots (Imtiaz et al. 2020), which causes performance degradation and higher error rates. To overcome these challenges, 3D OCDMA codes have emerged as a more scalable and flexible solution capable of increasing cardinality while maintaining practical feasibility (Nlend & Swart, 2023). Examples include the 3D Adaptive Cyclic-Shift / Multi-Diagonal Code, which replaces traditional wavelength and time with a dynamic cyclic shift sequence. Also, 3D-Single weight ZCC code (Alayedi et al. 2023) was derived by extending the 2D-SWZCC. Other distinguished contributions include the 3D multi-diagonal (3D-MD) code, which delivers absolute PIIN suppression, and hybrid schemes such as the 3D Perfect-Difference/Multi-Diagonal and 3D Perfect-Difference codes (Cherifi et al. 2023). While these codes offer improved performance, they often involve complex designs that limit practical implementation, especially for high-capacity, long-distance networks.

To address these gaps, the present study proposes a new 3-D FCC-MDW OCDMA system that integrates Flexible Cross-Correlation (FCC) and Modified Double-Weight (MDW) coding in the wavelength, time and spatial-domains. The objective of this work is to design and evaluate a robust, scalable 3-D code structure capable of supporting more simultaneous users while minimizing both MAI and PIIN effects. The proposed 3-D FCC-MDW code enhances system capacity, increases number of users, and supports has low optical received power at the receiver side.

The paper is organized as follows: Section 2 presents the complete 3-D FCC-MDW code construction, describing both the FCC and MDW architectural frameworks. Section 3 explains the methodology in detail, starting with the description of the proposed new class of 3-D FCC-MDW code, followed by the analysis of its cross-correlation properties, and concluding with the design of the MAI encoder/decoder architecture. Section 4 discusses the results, covering both the numerical evaluation and the simulation performance of the proposed system. Finally, Section 5 concludes the paper by summarizing the key findings and overall contributions of the research.

3-D FCC-MDW CODE CONSTRUCTION

The 3-D FCC-MDW code developed via extending an FCC and MDW OCDMA code into three dimensions: wavelength, time, and spatial. In this structure (Rahmani et al. 2022), every bit in the sequence has a corresponding time slot. Data transmission is indicated by the presence of a pulse, which is shown by a „1“ bit. A „0“ bit, on the other hand, indicates that there is no pulse and that no data is being transmitted during that time slot. This method is often used in basic digital communication to represent the flow of information. The 3-D FCC-MDW code is characterized by several unique properties: its wavelength M, time N, spatial length P, code length L, and weight w. The code also has a specific correlation function. The assigned sequence of the 3-D FCC-MDW is represented as a tuple $(L,w,\Lambda_a,\Lambda_c)$. Here, L indicates overall code length, calculated from the number of wavelengths (M), time domain (N), and space slots (P), Λ_a signifies autocorrelation and Λ_c represents the cross-correlation. The code exhibits several features: it is adaptable for high data throughput, its length enables efficient support of many concurrent users, and it allows for a simple system design.

FLEXIBLE CROSS-CORRELATION CODE (FCC)

The FCC code proposed by (Rashidi et al. 2014) is represented as A_K^W. As disclosed, a collection of non-zero components are created for flexible users and code length.

TABLE 1. FCC Code Architecture

(N,w,λ_{max})	N	K	w	Code Sequence
(9,4,1)	9	4	3	$\begin{pmatrix} 1 & 1 & 1 & 0 & 0 & 0 & 0 & 0 & 0 \\ 0 & 0 & 1 & 1 & 1 & 0 & 0 & 0 & 0 \\ 0 & 0 & 0 & 0 & 1 & 1 & 1 & 0 & 0 \\ 0 & 0 & 0 & 0 & 0 & 0 & 1 & 1 & 1 \end{pmatrix}$

The phase-shift correlation code with the shortest length is then obtained, where the code length is defined as:

$$Code\ Length = wK - \lambda_{max}(ith - 1) \quad (1)$$

Equation (1) represents flexible in-phase cross-correlation. These codes are distinguished by their minimum sequence length and number of active elements. For example, the FCC code can be designed as illustrated in Table 1.

1. Modified Double Weight Code (MDW)

   The MDW code has a weight that can be any even number greater than two (Morsy & Alsayyari, 2020). It is considered a family of Double Weight codes. In MDW, the basic matrix consists of two fundamental components:

Code length,

$$N_B = 3\sum_{j=1}^{\frac{w}{2}-1} j \quad (2)$$

and, total users,

$$K_B = \frac{w}{2} + 1 \quad (3)$$

Equation (2) and (3) represent the basic matrix of the MDW code (Din Keraf et al. 2014) with dimensions (K_B *x* N_B). Table 2 illustrates the architecture of MDW code for code length equal to nine.

TABLE 2. MDW Code Architecture

(N,w,λ_{max})	N	K_B	w	Code Sequence
(9,4,1)	9	3	4	$\begin{pmatrix} 0 & 0 & 0 & 0 & 1 & 1 & 0 & 1 & 1 \\ 0 & 1 & 1 & 0 & 0 & 0 & 1 & 1 & 0 \\ 1 & 1 & 0 & 1 & 1 & 0 & 0 & 0 & 0 \end{pmatrix}$

METHODOLOGY

NEW CLASS OF 3-D FCC-MDW CODE

The 3-D FCC-MDW code derived from FCC code where it utilizes the wavelength domain (U_f), and the transposed MDW codes (P_t^T), as the time domain. To further enhance system performance, the spatial domain (V_s), is incorporated using codewords with a weight of 2, as shown in Table 3. Each spatial codeword (e.g., v_0= [1 0 1]) activates two spatial positions, ensuring orthogonality among users and minimizing the spatial dimension. The addition of the spatial domain provides an extra layer of user separation, thereby increasing the total number of supported users while maintaining zero cross-correlation between spatial codes. Let the code sequence for the time domain by $P=\{p_0,p_1,\ldots\ldots p_{N-1}\}$, the wavelength domain be represented by $U=\{u_0,u_1,\ldots\ldots u_{M-1}\}$, and the spatial domain by $V=\{v_0,v_1,\ldots\ldots v_{P-1}\}$. Here U_f denotes the FCC wavelength encoding pattern, P_t represented the MDW time domain and V_s define the spatial code pattern.

TABLE 3. The 3-D FCC-MDW Sequences Across Wavelength, Time, and Spatial Domains

U_f	P_t^T	V_s
$u_0 = [1\ 1\ 1\ 0\ 0\ 0\ 0\ 0\ 0\ 0]$ $u_1 = [0\ 0\ 1\ 1\ 1\ 0\ 0\ 0\ 0\ 0]$ $u_2 = [0\ 0\ 0\ 0\ 1\ 1\ 1\ 0\ 0]$	$p_0 = \begin{bmatrix}1\\1\\0\end{bmatrix}$, $p_1 = \begin{bmatrix}0\\1\\1\end{bmatrix}$	$v_0 = [1\ 1\ 0]$ $v_1 = [0\ 1\ 1]$ $v_2 = [1\ 0\ 1]$

TABLE 4. The 3-D FCC-MDW code with parameters, $k_1 = 3$, $k_2 = 2$ and $k_3 = 2$

$\boldsymbol{u_0 = [1\ 1\ 1\ 0\ 0\ 0\ 0\ 0\ 0\ 0],\quad v_0 = [1\ 1\ 0]}$

$P_0 = \begin{bmatrix}1\\1\\0\end{bmatrix}$

$$\begin{bmatrix}1&1&1&0&0&0&0&0&0&0&1&1&1&0&0&0&0&0&0&0&0&0&0&0&0&0&0&0&0&0\\1&1&1&0&0&0&0&0&0&0&1&1&1&0&0&0&0&0&0&0&0&0&0&0&0&0&0&0&0&0\\0&0&0&0&0&0&0&0&0&0&0&0&0&0&0&0&0&0&0&0&0&0&0&0&0&0&0&0&0&0\end{bmatrix}$$

$P_1 = \begin{bmatrix}0\\1\\1\end{bmatrix}$

$$\begin{bmatrix}0&0&0&0&0&0&0&0&0&0&0&0&0&0&0&0&0&0&0&0&0&0&0&0&0&0&0&0&0&0\\1&1&1&0&0&0&0&0&0&0&1&1&1&0&0&0&0&0&0&0&0&0&0&0&0&0&0&0&0&0\\1&1&1&0&0&0&0&0&0&0&1&1&1&0&0&0&0&0&0&0&0&0&0&0&0&0&0&0&0&0\end{bmatrix}$$

$\boldsymbol{u_1 = [0\ 0\ 1\ 1\ 1\ 0\ 0\ 0\ 0],\quad v_0 = [1\ 1\ 0]}$

$P_0 = \begin{bmatrix}1\\1\\0\end{bmatrix}$

$$\begin{bmatrix}0&0&1&1&1&0&0&0&0&0&0&1&1&1&0&0&0&0&0&0&0&0&0&0&0&0&0&0&0&0\\0&0&1&1&1&0&0&0&0&0&0&1&1&1&0&0&0&0&0&0&0&0&0&0&0&0&0&0&0&0\\0&0&0&0&0&0&0&0&0&0&0&0&0&0&0&0&0&0&0&0&0&0&0&0&0&0&0&0&0&0\end{bmatrix}$$

$P_1 = \begin{bmatrix}0\\1\\1\end{bmatrix}$

$$\begin{bmatrix}0&0&0&0&0&0&0&0&0&0&0&0&0&0&0&0&0&0&0&0&0&0&0&0&0&0&0&0&0&0\\0&0&1&1&1&0&0&0&0&0&0&1&1&1&0&0&0&0&0&0&0&0&0&0&0&0&0&0&0&0\\0&0&1&1&1&0&0&0&0&0&0&1&1&1&0&0&0&0&0&0&0&0&0&0&0&0&0&0&0&0\end{bmatrix}$$

$P_0 = \begin{bmatrix}1\\1\\0\end{bmatrix}$

$\boldsymbol{u_2 = [0\ 0\ 0\ 0\ 1\ 1\ 1\ 0\ 0],\quad v_0 = [1\ 1\ 0]}$

$P_1 = \begin{bmatrix}0\\1\\1\end{bmatrix}$

$$\begin{bmatrix}0&0&0&0&1&1&1&0&0&0&0&1&1&1&0&0&0&0&0&0&0&0&0&0&0&0&0&0&0&0\\0&0&0&0&1&1&1&0&0&0&0&1&1&1&0&0&0&0&0&0&0&0&0&0&0&0&0&0&0&0\\0&0&0&0&0&0&0&0&0&0&0&0&0&0&0&0&0&0&0&0&0&0&0&0&0&0&0&0&0&0\end{bmatrix}$$

$$\begin{bmatrix}0&0&0&0&0&0&0&0&0&0&0&0&0&0&0&0&0&0&0&0&0&0&0&0&0&0&0&0&0&0\\0&0&0&0&1&1&1&0&0&0&0&1&1&1&0&0&0&0&0&0&0&0&0&0&0&0&0&0&0&0\\0&0&0&0&1&1&1&0&0&0&0&1&1&1&0&0&0&0&0&0&0&0&0&0&0&0&0&0&0&0\end{bmatrix}$$

$\boldsymbol{u_0 = [1\ 1\ 1\ 0\ 0\ 0\ 0\ 0\ 0\ 0],\quad v_1 = [0\ 1\ 1]}$

$P_0 = \begin{bmatrix}1\\1\\0\end{bmatrix}$

$$\begin{bmatrix}0&0&0&0&0&0&0&0&0&0&1&1&1&0&0&0&0&0&0&0&1&1&1&0&0&0&0&0&0&0\\0&0&0&0&0&0&0&0&0&0&1&1&1&0&0&0&0&0&0&0&1&1&1&0&0&0&0&0&0&0\\0&0&0&0&0&0&0&0&0&0&0&0&0&0&0&0&0&0&0&0&0&0&0&0&0&0&0&0&0&0\end{bmatrix}$$

$P_1 = \begin{bmatrix}0\\1\\1\end{bmatrix}$

$$\begin{bmatrix}0&0&0&0&0&0&0&0&0&0&0&0&0&0&0&0&0&0&0&0&0&0&0&0&0&0&0&0&0&0\\0&0&0&0&0&0&0&0&0&0&1&1&1&0&0&0&0&0&0&0&1&1&1&0&0&0&0&0&0&0\\0&0&0&0&0&0&0&0&0&0&1&1&1&0&0&0&0&0&0&0&1&1&1&0&0&0&0&0&0&0\end{bmatrix}$$

$\boldsymbol{u_1 = [0\ 0\ 1\ 1\ 1\ 0\ 0\ 0\ 0],\quad v_1 = [0\ 1\ 1]}$

$P_0 = \begin{bmatrix}1\\1\\0\end{bmatrix}$

$$\begin{bmatrix}0&0&0&0&0&0&0&0&0&0&0&0&1&1&1&0&0&0&0&0&0&0&1&1&1&0&0&0&0&0\\0&0&0&0&0&0&0&0&0&0&0&0&1&1&1&0&0&0&0&0&0&0&1&1&1&0&0&0&0&0\\0&0&0&0&0&0&0&0&0&0&0&0&0&0&0&0&0&0&0&0&0&0&0&0&0&0&0&0&0&0\end{bmatrix}$$

$P_1 = \begin{bmatrix}0\\1\\1\end{bmatrix}$

$$\begin{bmatrix}0&0&0&0&0&0&0&0&0&0&0&0&0&0&0&0&0&0&0&0&0&0&0&0&0&0&0&0&0&0\\0&0&0&0&0&0&0&0&0&0&0&0&1&1&1&0&0&0&0&0&0&0&1&1&1&0&0&0&0&0\\0&0&0&0&0&0&0&0&0&0&0&0&1&1&1&0&0&0&0&0&0&0&1&1&1&0&0&0&0&0\end{bmatrix}$$

continue...

...cont.

$P_0 = \begin{bmatrix}1\\1\\0\end{bmatrix}$	$u_2 = [0\ 0\ 0\ 0\ 1\ 1\ 1\ 0\ 0],\quad v_1 = [0\ 1\ 1]$
$P_1 = \begin{bmatrix}0\\1\\1\end{bmatrix}$	$\begin{bmatrix}0&0&0&0&0&0&0&0&0&0&0&0&0&1&1&1&0&0&0&0&0&0&1&1&1&0&0\\0&0&0&0&0&0&0&0&0&0&0&0&0&1&1&1&0&0&0&0&0&0&1&1&1&0&0\\0&0&0&0&0&0&0&0&0&0&0&0&0&0&0&0&0&0&0&0&0&0&0&0&0&0&0\end{bmatrix}$
	$\begin{bmatrix}0&0&0&0&0&0&0&0&0&0&0&0&0&0&0&0&0&0&0&0&0&0&0&0&0&0&0\\0&0&0&0&0&0&0&0&0&0&0&0&0&1&1&1&0&0&0&0&0&0&1&1&1&0&0\\0&0&0&0&0&0&0&0&0&0&0&0&0&1&1&1&0&0&0&0&0&0&1&1&1&0&0\end{bmatrix}$
	$u_0 = [1\ 1\ 1\ 0\ 0\ 0\ 0\ 0\ 0],\quad v_2 = [1\ 0\ 1]$
$P_0 = \begin{bmatrix}1\\1\\0\end{bmatrix}$	$\begin{bmatrix}1&1&1&0&0&0&0&0&0&0&0&0&0&0&0&0&0&0&1&1&1&0&0&0&0&0&0\\1&1&1&0&0&0&0&0&0&0&0&0&0&0&0&0&0&0&1&1&1&0&0&0&0&0&0\\0&0&0&0&0&0&0&0&0&0&0&0&0&0&0&0&0&0&0&0&0&0&0&0&0&0&0\end{bmatrix}$
$P_1 = \begin{bmatrix}0\\1\\1\end{bmatrix}$	$\begin{bmatrix}0&0&0&0&0&0&0&0&0&0&0&0&0&0&0&0&0&0&0&0&0&0&0&0&0&0&0\\1&1&1&0&0&0&0&0&0&0&0&0&0&0&0&0&0&0&1&1&1&0&0&0&0&0&0\\1&1&1&0&0&0&0&0&0&0&0&0&0&0&0&0&0&0&1&1&1&0&0&0&0&0&0\end{bmatrix}$
	$u_1 = [0\ 0\ 1\ 1\ 1\ 0\ 0\ 0\ 0],\quad v_2 = [1\ 0\ 1]$
$P_0 = \begin{bmatrix}1\\1\\0\end{bmatrix}$	$\begin{bmatrix}0&0&1&1&1&0&0&0&0&0&0&0&0&0&0&0&0&0&1&1&1&0&0&0&0&0&0\\0&0&1&1&1&0&0&0&0&0&0&0&0&0&0&0&0&0&1&1&1&0&0&0&0&0&0\\0&0&0&0&0&0&0&0&0&0&0&0&0&0&0&0&0&0&0&0&0&0&0&0&0&0&0\end{bmatrix}$
$P_1 = \begin{bmatrix}0\\1\\1\end{bmatrix}$	$\begin{bmatrix}0&0&0&0&0&0&0&0&0&0&0&0&0&0&0&0&0&0&0&0&0&0&0&0&0&0&0\\0&0&1&1&1&0&0&0&0&0&0&0&0&0&0&0&0&0&1&1&1&0&0&0&0&0&0\\0&0&1&1&1&0&0&0&0&0&0&0&0&0&0&0&0&0&1&1&1&0&0&0&0&0&0\end{bmatrix}$
	$u_2 = [0\ 0\ 0\ 0\ 1\ 1\ 1\ 0\ 0],\quad v_2 = [1\ 0\ 1]$
$P_0 = \begin{bmatrix}1\\1\\0\end{bmatrix}$	$\begin{bmatrix}0&0&0&0&1&1&1&0&0&0&0&0&0&0&0&0&0&0&0&0&1&1&1&0&0&0&0\\0&0&0&0&1&1&1&0&0&0&0&0&0&0&0&0&0&0&0&0&1&1&1&0&0&0&0\\0&0&0&0&0&0&0&0&0&0&0&0&0&0&0&0&0&0&0&0&0&0&0&0&0&0&0\end{bmatrix}$
$P_1 = \begin{bmatrix}0\\1\\1\end{bmatrix}$	$\begin{bmatrix}0&0&0&0&0&0&0&0&0&0&0&0&0&0&0&0&0&0&0&0&0&0&0&0&0&0&0\\0&0&0&0&1&1&1&0&0&0&0&0&0&0&0&0&0&0&0&0&1&1&1&0&0&0&0\\0&0&0&0&1&1&1&0&0&0&0&0&0&0&0&0&0&0&0&0&1&1&1&0&0&0&0\end{bmatrix}$

The 3-D FCC-MDW can be designed with the following properties: -

$$A_{f,t,s} = U_f P_t^T V_s \tag{4}$$

where, $t = \{1, 2, \ldots\ldots, N-1\}$, $f = \{1, 2, \ldots\ldots, M-1\}$, and $s = \{1, 2, \ldots\ldots, P-1\}$.

Table 4 clearly demonstrates the 3-D FCC-MDW sequence for $k_1 = 3$, $k_2 = 2$ and $k_3 = 2$, where k_1, k_2 and k_3 represent the assigned weights of the sequences U_f, P_t and V_s.

3-D FCC-MDW CROSS-CORRELATION

The properties of 3-D FCC-MDW codes cross correlation are determined using eight characteristic matrices(Yasmin et al. 2020), $A^{(q)}$, where q = 0,1,2,… ,7. These matrices facilitate a clear characterization of the code's correlation properties as follows:

$$A^{(q)} = \begin{cases} UP^TV \\ \overline{U}P^TV \\ UP^T\overline{V} \\ \overline{U}P^T\overline{V} \end{cases} \text{ and } \begin{cases} UP^T\overline{V} \\ \overline{U}P^T\overline{V} \\ U\overline{P}^TV \\ \overline{U}\overline{P}^TV \end{cases} \tag{5}$$

The sequences U, P and V and their complements are $\overline{U}$, $\overline{P}$ and $\overline{V}$. Suppose, U = [001110000], then its complement $\overline{U}$ is obtained by inverting each element of U, i.e., U= [110001111]. Correlation function of 3-D FCC-MDW sequence $A^{(q)}$ and $A_{f,t,s}$ is expressed:

$$R^{(q)}(f,t,s) = \sum_{i=0}^{M-1}\sum_{j=0}^{N-1}\sum_{l=0}^{P-1} a_{i,j,l}^{(d)}\, a_{(i+f)(j+t)(l+s)} \tag{6}$$

where $a_{i,j,t}^{(q)}$ represent the code martrix $A^{(q)}$, $a_{(i+f)(j+t)(l+s)}$ denotes the corresponding element in $A_{f,t,s}$. Correlation analysis of the chosen codes, $A^{(q)}$ and $A_{f,t,s}$, are summarized in Table 5 for the developed 3-D FCC-MDW code structure. The correlation metrics of the 3-D FCC-MDW code, as determined by the provided equation:

$$R^{(0)}(f,t,s) - \frac{R^{(1)}(f,t,s)}{k_1-1} - \frac{R^{(2)}(f,t,s)}{k_2-1} + \frac{R^{(3)}(f,t,s)}{k_1-1} = \begin{cases} k_1k_2k_3, & for\ f=0,t=0,s=0 \\ k_1k_2, & for\ f=0,t=0,s\neq 0 \\ 0, & otherwise \end{cases} \quad (7)$$

TABLE 5. The 3-D FCC-MDW Cross-Correlation Properties

Case condition	Non-zero correlation terms
$f=0,t=0,s=0$	$R^{(0)}=(k_1k_2k_3)$
Single offset (only one of $f,t,s\neq 0$)	$R^{(0)}=(k_1k_3),\ R^{(2)}=(k_2-1)(k_1k_3)$ $R^{(0)}=(k_2k_3),\ R^{(1)}=(k_1-1)(k_2k_3)$ $R^{(0)}=(k_1k_2),\ R^{(4)}=(k_3-1)(k_1k_2)$
Dual Offset (two of $f,t,s\neq 0$)	$R^{(0)}=k_1,\ R^{(2)}=(k_2-1)(k_1),\ R^{(4)}=(k_3-1)(k_1)$ $R^{(0)}=k_2,\ R^{(1)}=(k_1-1)(k_2),\ R^{(5)}=(k_3-1)(k_2)$ $R^{(0)}=k_3,\ R^{(1)}=(k_1-1)(k_3),\ R^{(2)}=(k_2-1)(k_3)$
Triple Offset ($f\neq 0,t\neq 0,s\neq 0$)	$R^{(0)}=1,\ R^{(1)}=(k_1-1),\ R^{(2)}=(k_2-1),\ R^{(3)}=(k_1-1),$ $R^{(4)}=(k_3-1),\ R^{(5)}=(k_1-1)(k_3-1),\ R^{(6)}=(k_1-1)(k_2-1),\ R^{(7)}=(k_1-1)(k_2-1)\ (k_3-1)$
All other conditions	$R^{(i)}=0$

Similarly, observing Table 5, we obtain.

$$R^{(4)}(f,t,s) - \frac{R^{(5)}(f,t,s)}{k_1-1} - \frac{R^{(6)}(f,t,s)}{k_2-1} + \frac{R^{(7)}(f,t,s)}{(k_1-1)(k_2-1)} = \begin{cases} k_1k_2(k_3-1), & for\ f=0,t=0,s\neq 0 \\ 0, & otherwise \end{cases} \quad (8)$$

Based on the properties expressed in equation (7) and (8), the system exhibits a MAI cancellation property as follows:

$$R^{(0)}(f,t,s) - \frac{R^{(1)}(f,t,s)}{k_1-1} - \frac{R^{(2)}(f,t,s)}{k_2-1} + \frac{R^{(3)}(f,t,s)}{k_1-1} - \frac{1}{k_3-1}\left[R^{(4)}(f,t,s) - \frac{R^{(5)}(f,t,s)}{k_1-1} - \frac{R^{(6)}(f,t,s)}{k_2-1} + \frac{R^{(7)}(f,t,s)}{(k_1-1)(k_2-1)}\right] = \begin{cases} k_1k_2k_3, & for\ f=0,t=0,s=0 \\ 0, & otherwise \end{cases} \quad (9)$$

MAI ENCODER/DECODER DESIGN

The En/Decoder design regarding the 3-D FCC-MDW code shown in Figure 1. Enc/Decoder uses a total number of weights, w = $k_1 \times k_2 \times k_3$, and each encoder and decoder operate with a unique codeword. Each encoder has a broadband light source and an external modulator (MZM), which transforms the electrical signal within optical. These modulated optical signals are then routed through an optical switch, which selects wavelengths allowing the spectral code sequence, U_f. The output is passed through a set of optical delay lines that apply specific time delays based on the time-domain code P_t. The delayed signals are then sent to several output ports across spatial coordinates V_s employing a splitter, where each output line is coupled to a separate coupler for transmission. In the encoding process, the input data is first modulated by the MZM into optical pulses. After that, these pulses pass through an optical switch, which uses the specified spectral code to choose the right wavelengths. The 3-D code structure is implemented by first passing the spectrally encoded signal through optical delay lines for time encoding and then using a splitter to disperse it across several spatial routes.

Figure 2 shows the corresponding decoder structure, which includes an optical combiner, multiple correlators, and balanced detectors. Optical signals from different spatial couplers are first combined based on the spatial code V_s. The combined signal is then split and fed into two correlators for time-domain decoding using both the original time code P_t and its compliments P_t. The outputs from these correlators are directed to balanced detectors. Each balanced detector includes optical switches to reverse the wavelength encoding according to U_f, dual photodetectors, and power adjustment circuits to normalize signal intensity. The spectral decoding process at the receiver mirrors the encoding process used in the encoder.

The outputs from the upper and lower arms of the decoder correspond to various correlation components of the received signal. The use of balanced detection, supported by the structure of the 3D FCC-MDW code and spatial domain processing, substantially increases the ratio of signal power to noise, reducing interference from non-desired users.

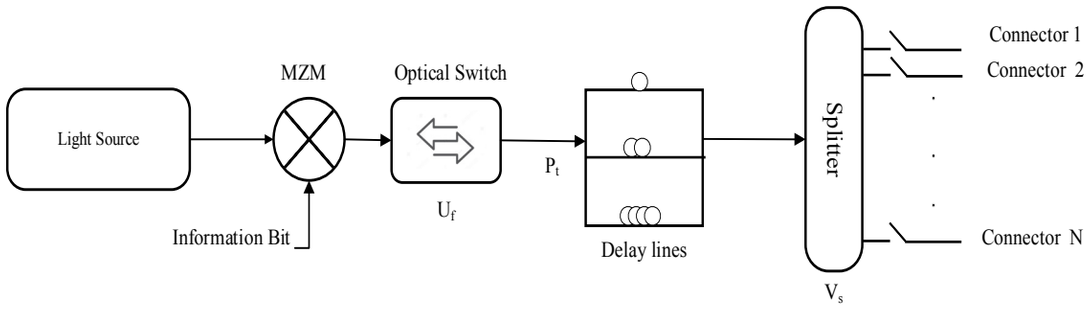

FIGURE 1. The 3-D FCC-MDW Encoder Structure

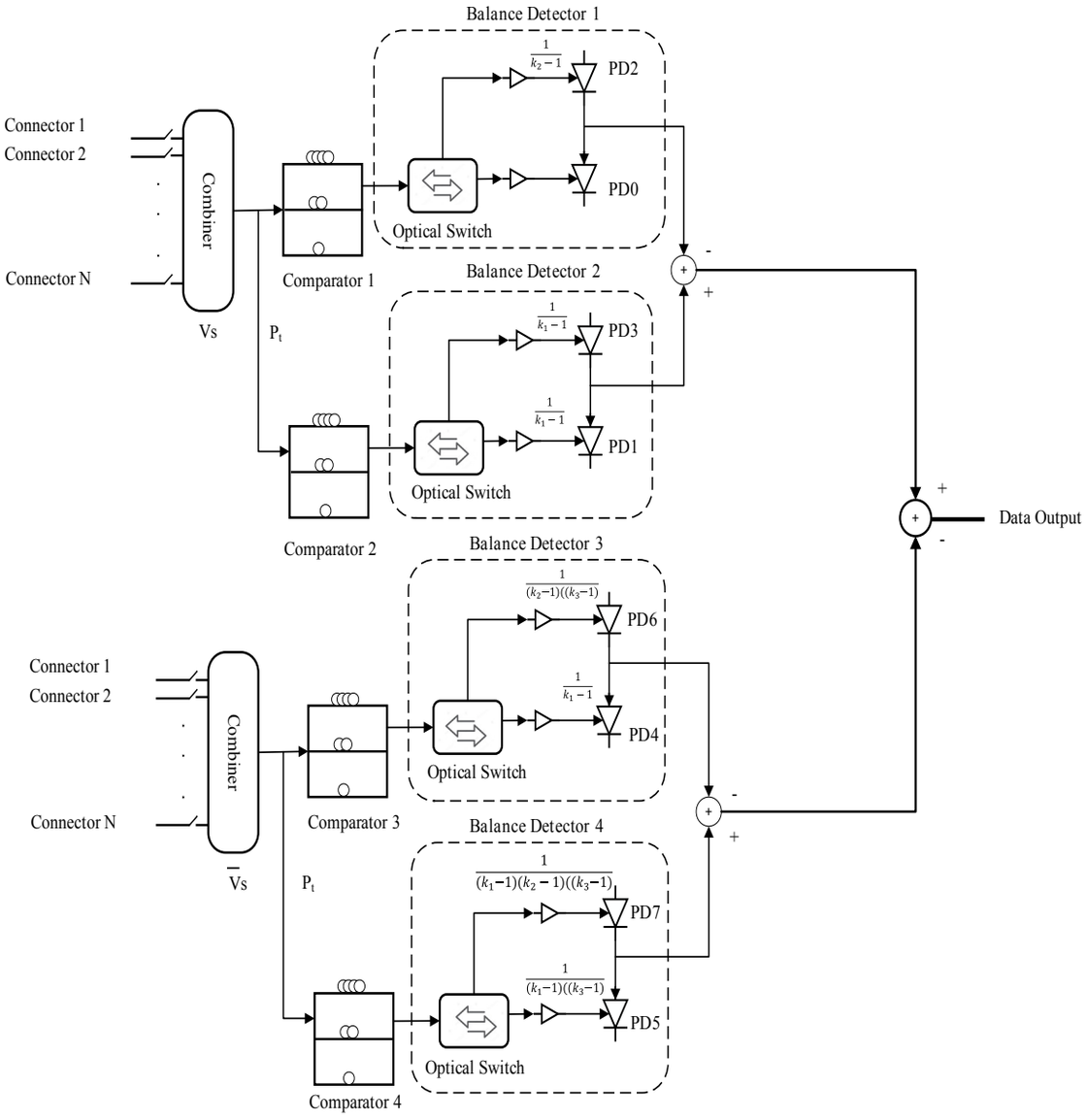

FIGURE 2. The 3-D FCC-MDW Decoder Structure

RESULTS AND DISCUSSION

PERFORMANCE ANALYSIS

In this paper, the 3-D FCC-MDW code is evaluated under the influence of various noise sources. Specifically, three major types of noise are considered: thermal noise, which arises caused by the unpredictable behaviour of electrons in the receiving circuitry; shot noise, which is linked to the discrete nature of photon detection; and PIIN, which results from the beating of optical fields with random phase variations. To accurately assess system performance, BER is evaluated using the Gaussian evaluation method, as outlined by (Anuar et al. 2024). Thus, the general expression for the photocurrent noise produced by the Photodetectors is given by:

$$i_{noise}^2 = i_{PIIN}^2 + i_{shot}^2 + i_{thermal}^2 = BI^2\tau_c + 2eI_{total}B + \frac{4K_bT_nB}{R_L} \quad (10)$$

The expression includes several key variables: B denotes the system's electrical bandwidth, I denotes the mean photocurrent, and e is the elementary current flow of an electron. K_b is the Boltzmann constant (Boukricha et al. 2020), T_n denotes the noise of the receiver, R_L refers to the load resistance and τ_c is the correlation time of Photodetector and given:

$$\tau_c = \frac{\int_0^\infty H_0^2(x)dx}{(\int_0^\infty H_0(x)dx)^2} \quad (11)$$

The analysis is based on several key assumptions. First, an incoherent broadband light source, $H_o(x)$ with a flat spectrum is employed, implying that the optical power is uniformly distributed across the source bandwidth, centred at the optical carrier frequency. Second, it is assumed that each spectral component has a similar spectral width. Third, all users are allocated an equal share of the transmitted optical power. Finally, the users' bit streams are perfectly synchronized (Kumari & Bansal, 2023). The correlation across codewords $A^{(q)}$ and $A_{f,t,s}$ to derive the output currents of PSs 0 through 7, which is given by:

$$I_{(PS/0\sim7)} = \Re \int_0^\infty H_{(0\sim7)}(x)dx \quad (12)$$

where Equation (12) is photo-detector sensitivity. The corresponding average photocurrent at the receiver can be expressed as:

$$= \frac{\Re P_{ST}K_1}{M} \quad (13)$$

The variance of the PIIN current is given by the following equation:

$$i_{PIIN}^2 = \frac{MB}{2\Delta_x}\left\{\frac{(I_0-I_2-I_4+I_6)^2}{K_1} + \frac{(I_1-I_3-I_5+I_7)^2}{(K_1-1)^2}\right\} \quad (14)$$

The shot noise originating from photodetectors (PSs) 0 through 7 are independent of each other and is characterized by formulation:

$$i_{shot}^2 = 2eI_{total}B = 2eB\sum_{i=0}^{7} I_i$$

]If '0' and '1' are sent equally probability for each other, the equation is equivalent to,

$$i_{shot}^2 = eB\sum_{i=0}^{7} I_i \quad (15)$$

The expression for thermal noise is:

$$i_{thermal}^2 = \frac{4K_bT_nB}{R_L} \quad (16)$$

From the equations (13), (14), (15) and (16) the SNR at Receiver are as follows:

$$SNR = \frac{I^2}{i_{PIIN}^2+i_{shot}^2+i_{thermal}^2} = \frac{\left\{\frac{\Re P_{ST}K_1}{M}\right\}^2}{\frac{MB}{2\Delta_x}\left\{\frac{(I_0-I_2-I_4+I_6)^2}{K_1}+\frac{(I_1-I_3-I_5+I_7)^2}{(K_1-1)^2}\right\}+eB\sum_{i=0}^{7} I_i+\frac{4K_bT_nB}{R_L}} \quad (17)$$

Based on the gaussian approximation, the bit error rate is given by (Cherifi et al. 2021)

$$BER = \frac{1}{2}erfc\left(\sqrt{\frac{SNR}{8}}\right) \quad (18)$$

The effectiveness of the 3-D FCC-MDW code is numerically compared with existing OCDMA codes, including 3D-MD, 3D-SWZCC, 3D-VWZCC and 2-D FCC-MDW. The numerical analysis for these calculations is mentioned in Table 6.

Figure 3 illustrates the comparison of BER against user count for different OCDMA codes at a fixed bit rate

of, R_b=1.25 Gbps and received optical signal power of, P_{sr}=-10 dBm. The designed 3-D FCC-MDW code clearly outperforms the other systems. At BER of 10^{-9}, the 3-D FCC-MDW supports up to 310 users, compared to only 80 users for 3D-MD, 60 users for 3D-VWZCC, and 100 users for 3D-SWZCC. This represents a user-capacity improvement of nearly 3.9 times over 3D-MD, 5.2 times over 3D-VWZCC, and 3.1 times over 3D-SWZCC. The ability of the proposed system to maintain very low BER, even under high user load, confirms its superior performance in suppressing MAI and mitigating PIIN, thanks to its flexible and low cross-correlation code structure across the wavelength, time, and spatial domains.

TABLE 6. Performance Evaluation Metrics

Parameter	Value
Photodetector sensitivity, $(\Re)$	0.75
Optical spectrum width, (Δx)	3.75 THz
Bit rate, (R_b)	1.25 Gbps
Electrical Bandwidth, (B)	$R_b/_2$
Elementary charge, (e)	1.602×10^{-19} C

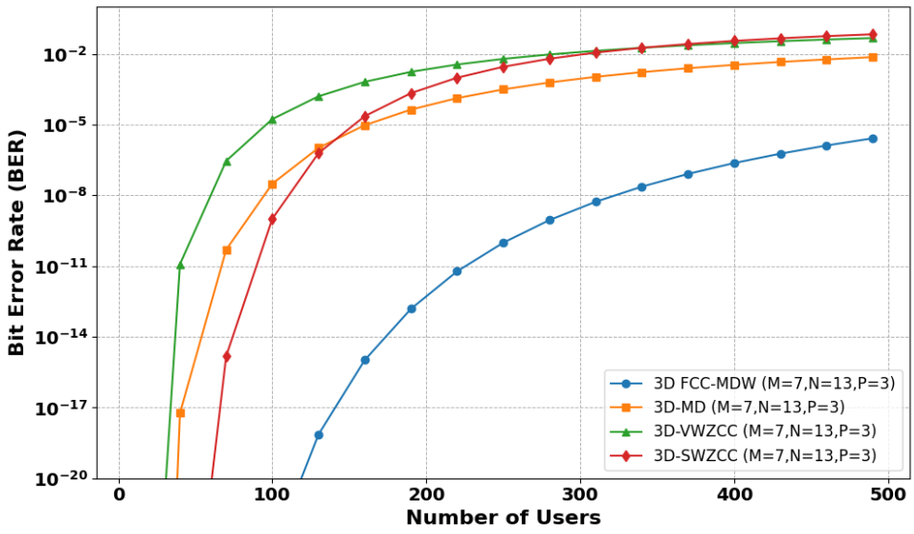

FIGURE 3. Effect of BER for Various OCDMA Codes

Figure 4 represents the plots depicting the relationship between received optical power and BER for the 3-D FCC-MDW, 3D- SWZCC, 3D-MD, and 2-D FCC-MDW code families using a bit rate of, R_b=1.25 Gbps. The optical received power, P_{sr}, ranges from -37 dBm to 5 dBm. At a BER of 10^{-9}, the 3-D FCC-MDW code achieves the most effective optical received power of -24 dBm. In comparison, the corresponding values for the 3D- MD, 2-D FCC-MDW, and 3D-SWZCC codes are -22 dBm, -18 dBm, and -15 dBm, respectively. This results in optical received power edge of approximately 2 dBm, 6 dBm, and 9 dBm relative to the 3-D FCC-MDW code. Consequently, in contrast to the other code families, the 3-D FCC-MDW sequence is thought to be the best scheme in this situation since it needs the least amount received power to achieve reliable performance at the photodetector compared with the other code families.

Figure 5 shows how various code weight configurations in the proposed 3-D FCC-MDW code impact system capacity and displays the performance analysis. In lightweight configurations, such as weights (2,1,2) and (2,2,1), the BER threshold of 10^{-9}, is reached at approximately 310 users, indicating limited acceptance to multiple-access interference. Balanced-weight configurations, including (3,4,2) and (3,3,3), increase this limit, supporting roughly 370-400 users before exceeding the threshold. In contrast, dense-weight configurations, such as (4, 2, 2) and (3, 2, 2), keep BER values well below

10^{-9} even when the number of users approaches 430 above. This indicates much better performance and higher resistance to multiple-access interference in the proposed 3-D FCC-MDW code. The improved power of these higher-weight codes in the proposed scheme comes from having more active chips per codewords, which helps to reduce the minimal interference, cross-correlation properties, and maintaining bit error rates even under heavy user loads.

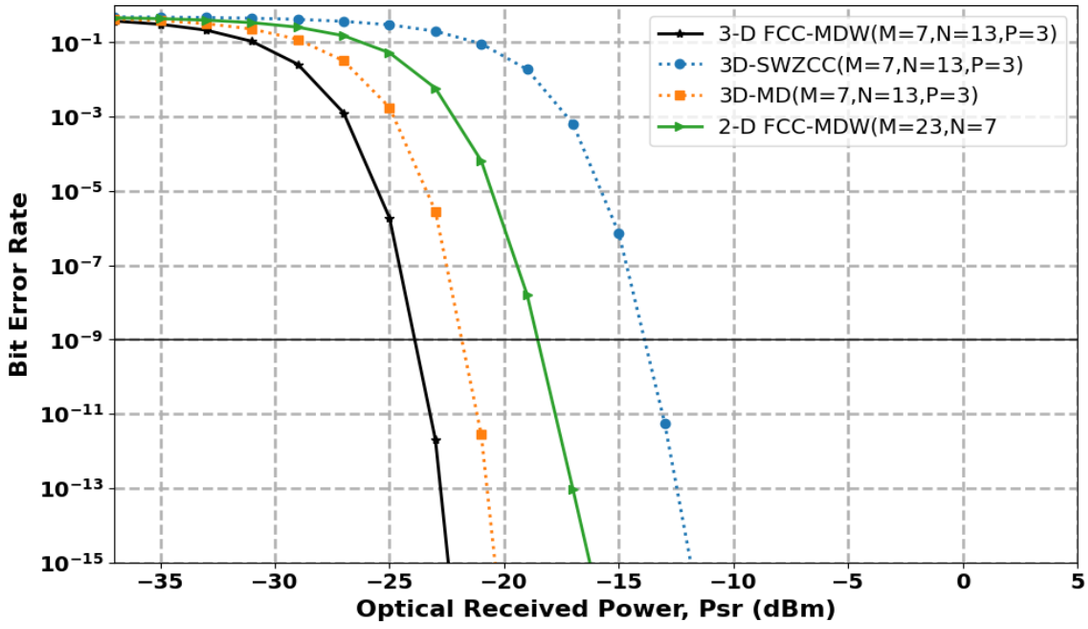

FIGURE 4. Effect of Optical Received Power vs. BER for Various OCDMA Codes

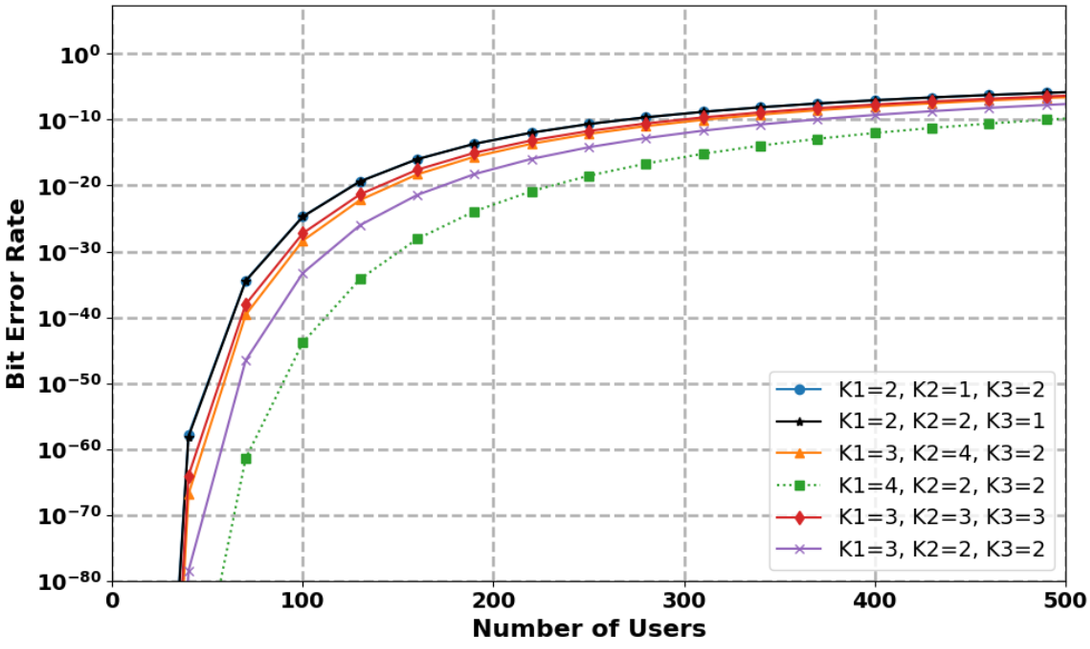

FIGURE 5. Effect of BER versus Number of Users for Various Weight Schemes

Figure 6 plots BER with respect to Spectral width (Δx) in THz, with P_{sr} = –10 dBm and a bit rate of R_b=1.25 Gbps. It can be observed that the proposed 3-D FCC-MDW code achieves a BER below 10^{-9} with an only 0.084 THz. The 3D-MD, 3D-SWZCC, and 2-D FCC-MDW, the codes require an extensive spectral range, reaching 5.67 THz, 0.14 THz, and 4.5 THz. Therefore, the proposed 3-D FCC-MDW code shows the superior spectral efficiency by requiring the smallest spectral width between the compared coding schemes.

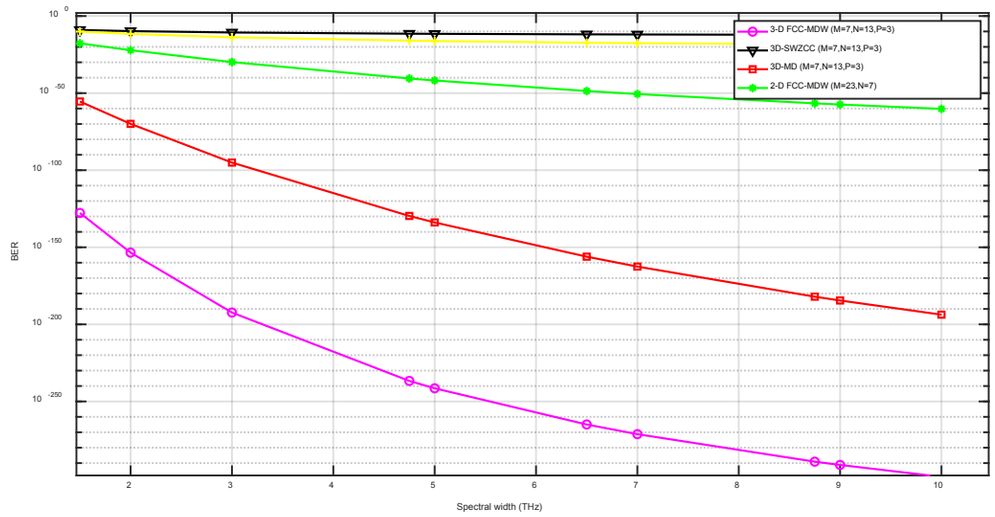

FIGURE 6. Effect of BER versus Spectral Width for Various OCDMA Codes

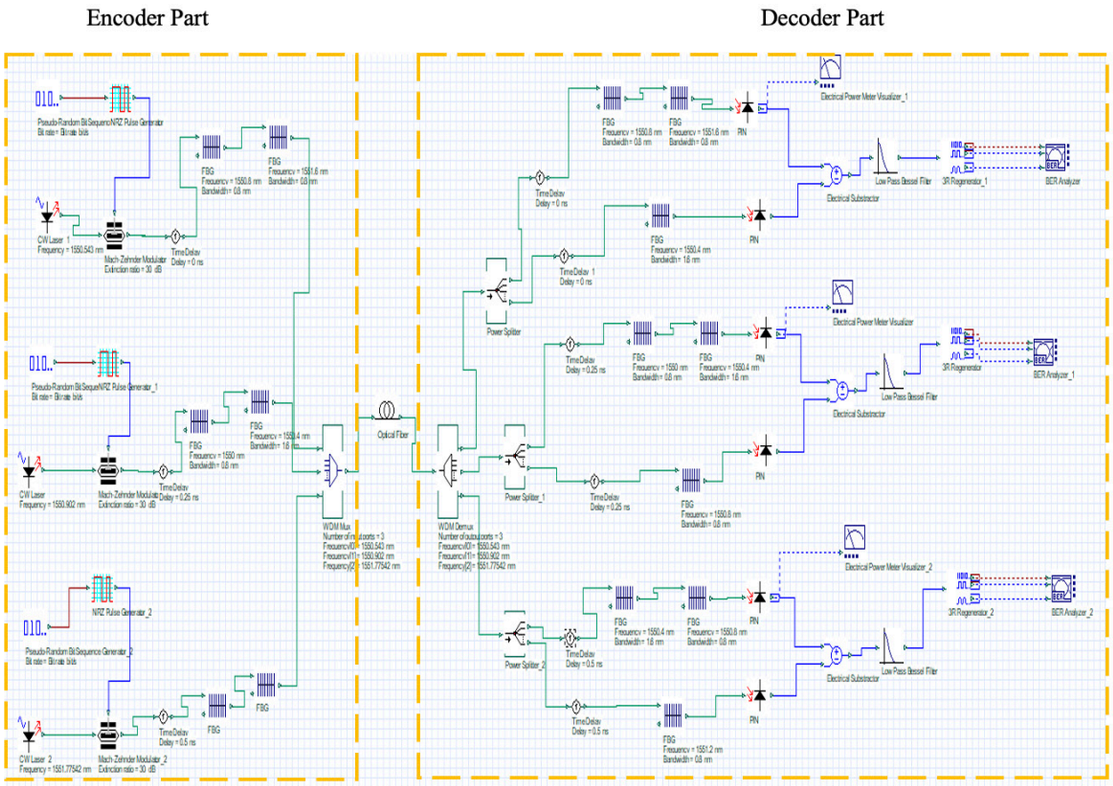

FIGURE 7. The 3-D FCC-MDW En/Decoder Design for 3-Users

SIMULATION ANALYSIS

Simulations of the proposed setup were carried out using OptiSystem 21.0. with three active users, where each user's data is encoded across the wavelength, time, and spatial domains, as shown in Figure 7. The transmitter of the 3-D FCC-MDW system consists of a CW laser as the optical source along with a Pseudo-Random Bit Sequence (PRBS) generator and a pulse generator to format the electrical data. Electro-optic modulator MZM converts the electrical signals into optical pulses. Fiber Bragg Gratings (FBGs) are employed for spectral encoding, while time delays are used for time-domain encoding. In the spatial domain, power splitters and combiners share and join optical signals across several spatial paths, giving an extra way to carry out 3-D encoding. The encoded signals from all three users are then combined using a wavelength division multiplexer (WDM-Mux) and transmitted through an optical fiber. At the receiver part, a WDM demultiplexer separates the wavelengths, and power splitters direct the signals into the appropriate decoding branches. Power splitters then send these signals into their matching decoding paths. Fiber Bragg Gratings (FBGs) and time delays are used in each path to extract the original data, while power splitters and combiners are employed to decode the spatial part. Low-pass Bessel filters remove unwanted noise, and electrical subtractors minimize interference. Finally, a 3R regenerator restores the signal before Bit error rate analysis.

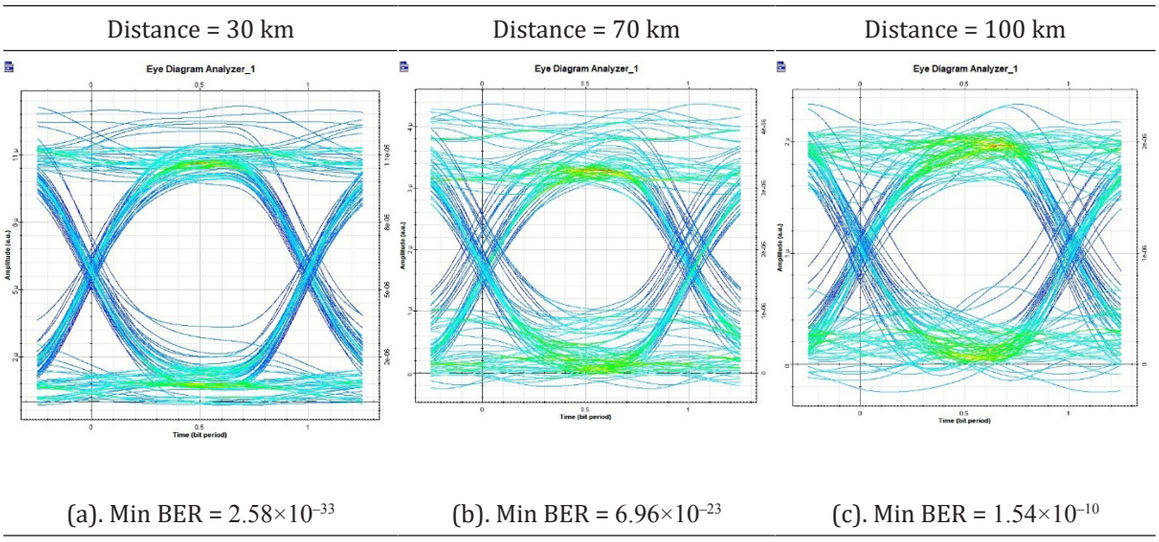

FIGURE 8. The 3-D FCC-MDW Eye Diagrams for Fiber Length at Different Distances

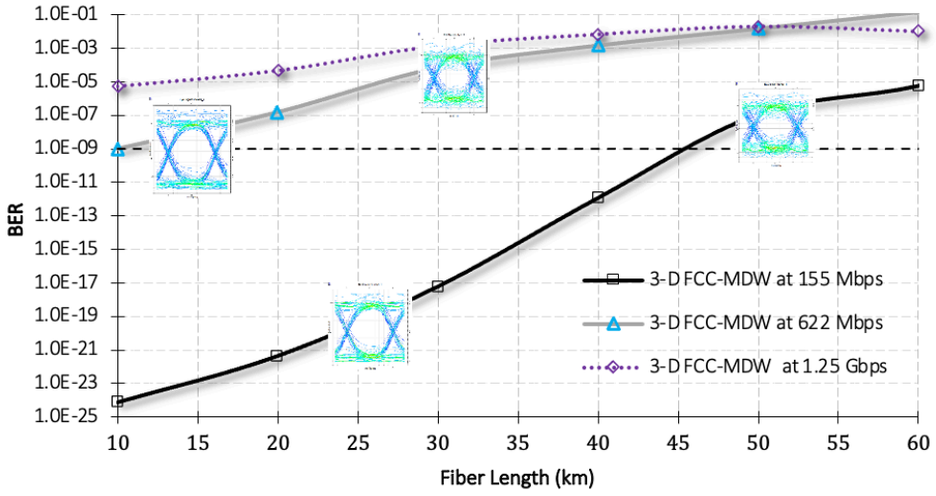

FIGURE 9. Effect of BER over Fiber Length at Different Bit Rates for the 3-D FCC-MDW Code

Figure 9 represents BER performance versus distances at data transmission rates of 155 Mbps, 622 Mbps, and 1.25 Gbps At performance BER of 10^{-9}, the system can transmit reliably up to about 52 km at 155 Mbps, 28 km at 622 Mbps, and 12 km at 1.25 Gbps. When the bit rate increases, the BER worsens faster with distance, and the eye diagrams become narrower at higher bit rates. However, by sustaining error-free operation at lower bit rates over longer spans and offering satisfactory detection at higher bit rates, the 3-D FCC-MDW code exhibits strong performance. These results confirm that the coding provides a good balance between data throughput and transmission distance and effectively lowers PIIN and MAI for OCDMA systems.

Figure 10 demonstrates the BER performance of the system with respect to back-to-back (B2B) effective optical received power (P_{sr}). The plot accounts for three major types of disturbances affecting the system are PIIN, photon-counting noise, and thermal-induced noise. The optical received power (Psr) range is from –33 dBm to –11 dBm, and the discrepancy between the numerical and simulation results is approximately –6 dBm. The variation is primarily due to the difficulty of maintaining a fixed effective received power in simulations, a factor that is assumed to be constant in theoretical analysis. Additionally, the simulation model incorporates real-world impairments like insertion losses, pulse broadening and nonlinear phase modulation which are not accounted for in theoretical calculations.

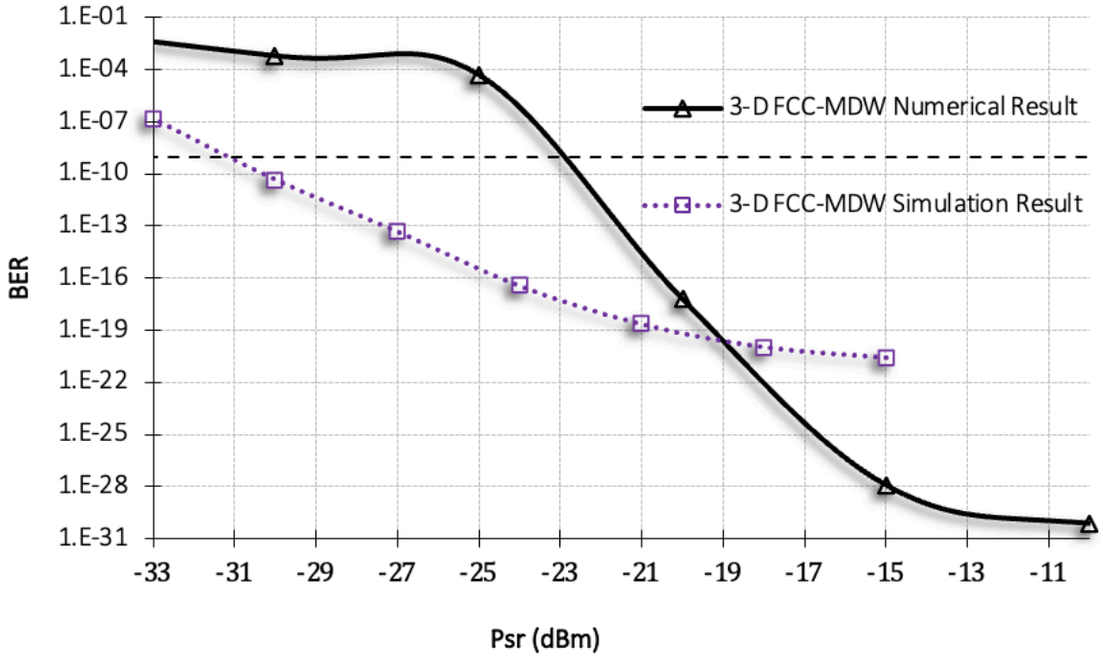

FIGURE 10. Validation of BER versus Optical Received Power for the 3-D FCC-MDW code]

CONCLUSION

The paper explores and evaluates the development of a new 3-D FCC-MDW code for OCDMA systems, developed to improve interference resistance, user capacity and spectral efficiency. The simulation results confirm that the proposed system offers substantial enhancements compared to traditional 2-D and 3-D code families. At a fixed bit rate R_b=1.25 Gbps and optical received power of P_{sr} = – 10 dBm, the 3-D FCC-MDW supports up to 310 users at BER ≤ 10^{-9}, outperforming 3D-MD, 3D-VWZCC, and 3D-SWZCC by factors of 3.9 times, 5.2, and 3.1 times, respectively. In optical power analysis, the system demonstrates superior efficiency, requiring the lowest received power -24 dBm to achieve reliable detection relative to other codes. The flexibility of the suggested code is further demonstrated by weight configuration analysis, which shows that denser weight configurations may support over 430 users with minimal probability and strong scalability. The 3-D FCC-MDW also proves highly spectrally efficient, requiring only 0.084 THz bandwidth to maintain BER below 10^{-9}, far less than other schemes. The transmission performance over single-mode fiber

(SMF) was also evaluated. The results allow data transmission through the proposed code maximum of 52 km at 155 Mbps, 28 km at 622 Mbps, and 12 km at 1.25 Gbps with a BER below 10^{-9}. As the bit rate increases, BER worsens faster due to dispersion and attenuation, and the eye diagrams become narrower. Still, the system achieves error-free operation at lower rates over longer distances and maintains good detection at higher rates. This confirms that the 3-D FCC-MDW code provides a strong balance between speed and distance while reducing PIIN and MAI.

ACKNOWLEDGEMENT

The authors are grateful for the financial support by Academy of Medical Sciences Networking Grants Scheme under the grant number (NGR\1560)

DECLARATION OF COMPETING INTEREST

None.

REFERENCES

Alayedi, M., Cherifi, A., Hamida, A. F., Matem, R. & El-Mottaleb, S. A. A. 2023. Performance improvement of SAC-OCDMA network utilizing an identity column shifting matrix (ICSM) code. 263–278. https://doi.org/10.1007/978-3-031-21101-0_21

Alayedi, M., Jaradat, A. M., Elgammal, Z. & Malkawi, M. 2024. Performance optimization of SAC-OCDMA network based on 2-D CS code utilizing two light sources. 2024 6th International Symposium on Advanced Electrical and Communication Technologies (ISAECT): 1–6. https://doi.org/10.1109/ISAECT64333.2024.10799858

Aljunid, S. M. A., Anuar, M. A., Ismail, A. A. M., Keraf, N. D., Matem, R., Rashidi, C. B. M., Ali, N., Amirul, M. S., Endut, R. & Hambali, N. A. M. A. 2021. Two dimensional (2D) OCDMA encoder/decoder for various industrial application. *International Journal of Nanoelectronics and Materials* 14(Special Issue InCAPE): 175–182.

Anuar, M. A., Ammar, S. M., Aljunid, S. A., Ali, N., Endut, R. & Saad, N. M. 2024. Optimizing bit error rate in optical CDMA systems via flexible double weight code implementation. 2024 IEEE 1st International Conference on Communication Engineering and Emerging Technologies (ICoCET): 1–4. https://doi.org/10.1109/ICoCET63343.2024.10730485

Boukricha, S., Ghoumid, K., Mekaoui, S., Ar-Reyouchi, E., Bourouina, H. & Yahiaoui, R. 2020. SAC-OCDMA system performance using narrowband Bragg filter encoders and decoders. *SN Applied Sciences* 2(6): 1002. https://doi.org/10.1007/s42452-020-2700-9

Cherifi, A., Bouazza, B. S., Alayedi, M., Aljunid, S. A. & Rashidi, C. B. M. 2021. Development and performance improvement of a new two-dimensional spectral/spatial code using the Pascal triangle rule for OCDMA system. *Journal of Optical Communications* 42(1): 149–158. https://doi.org/10.1515/joc-2018-0052

Cherifi, A., Mohammed Chikouche, T., Karar, A. S., Barakat, J. M. H., Arbouche, O. & Dayoub, I. 2023. Capacity improvement of 3D-OCDMA-PON hybrid system next generation using weight zero cross correlation code. *Applied Sciences* 13(10). https://doi.org/10.3390/app13105869

Din Keraf, N., Aljunid, S. A., Arief, A. R., Anuar, M. S., Rashidi, C. B. M., Ehkan, P. & Nurol, M. N. 2014. An optimal cardinality of wavelength/time incoherent OCDMA system using 2-D hybrid FCC-MDW code. 2014 2nd International Conference on Electronic Design (ICED): 356–361. https://doi.org/10.1109/ICED.2014.7015830

Imtiaz, W. A., Ahmed, H. Y., Zeghid, M. & Sharief, Y. 2020. An optimized architecture to reduce the impact of fiber strands in spectral/spatial optical code division multiple access passive optical networks (OCDMA-PON). *Optical Fiber Technology* 54: 102072. https://doi.org/10.1016/j.yofte.2019.102072

Kumari, M. & Bansal, S. 2023. Inter-satellite OWC incorporated OCDMA system employing modified ZCC code. 2023 IEEE 3rd Mysore Sub Section International Conference (MysuruCon): 1–6. https://doi.org/10.1109/MysuruCon59703.2023.10397010

Liang, L., Zhang, S., Li, J., Plaza, A. & Cui, Z. 2023. Multi-scale spectral-spatial attention network for hyperspectral image classification combining 2D octave and 3D convolutional neural networks. *Remote Sensing* 15(7): 1758. https://doi.org/10.3390/rs15071758

Mizozoe, K., Matsumoto, T., Ohira, Y., Torii, H. & Ida, Y. 2023. Study on robustness to optical diffusion on undersea optical CDMA system using 2D optical ZCZ sequences. 2023 IEEE 12th Global Conference on Consumer Electronics (GCCE): 1090–1094. https://doi.org/10.1109/GCCE59613.2023.10315397

Morsy, M. A. & Alsayyari, A. S. 2020. Performance analysis of incoherent PPM - OCDMA networks based on optimised modified prime code for multimedia applications. *IET Communications* 14(22): 4014–4021. https://doi.org/10.1049/iet-com.2020.0155

Nlend, S. & Swart, T. G. 2023. Multiple access interference

bit error rate evaluation technique for direct detection FFH-OCDMA Bragg gratings based channels. *ECTI Transactions on Electrical Engineering, Electronics, and Communications* 21(3): 251467. https://doi.org/10.37936/ecti-eec.2023213.251467

Rahmani, M., Cherifi, A., Sabri, G. N., Bouazza, B. S. & Karar, A. 2022. Contribution of OFDM modulation to improve the performance of non-coherent OCDMA system based on a new variable weight zero cross correlation code. *Optical and Quantum Electronics* 54(9): 576. https://doi.org/10.1007/s11082-022-03949-5

Rashidi, C. B. M., Aljunid, S. A., Ghani, F., Fadhil, H. A., Anuar, M. S. & Arief, A. R. 2014. Cardinality enrichment of flexible cross correlation (FCC) code for SAC-OCDMA system by alleviation interference scheme (AIS). *Optik* 125(17): 4889–4894. https://doi.org/10.1016/j.ijleo.2014.04.035

Yasmin, N., Islam, M. J. & Islam, M. R. 2020. Performance of fiber optic MW-OCDMA system in presence of XPM effect. 2020 2nd International Conference on Advanced Information and Communication Technology (ICAICT): 364–369. https://doi.org/10.1109/ICAICT51780.2020.9333486